

A Rigid Mid-Lift-to-Drag Ratio Approach to Human Mars Entry, Descent, and Landing

Christopher J. Cerimele¹, Edward A. Robertson², Ronald R. Sostaric³(editor), Charles H. Campbell⁴, Phil Robinson⁵,
Daniel A. Matz⁶, Breanna J. Johnson⁷, Susan J. Stachowiak⁸
NASA Johnson Space Center, Houston, TX, 77058

Joseph A. Garcia⁹, Jeffrey V. Bowles¹⁰, David J. Kinney¹¹
NASA Ames Research Center, Moffet Field, CA, 94035

and

John E. Theisinger¹²
NASA Langley Research Center, Hampton, VA, 23681

Current NASA Human Mars architectures require delivery of approximately 20 metric tons of cargo to the surface in a single landing. A proposed vehicle type for performing the entry, descent, and landing at Mars associated with this architecture is a rigid, enclosed, elongated lifting body shape that provides a higher lift-to-drag ratio (L/D) than a typical entry capsule, but lower than a typical winged entry vehicle (such as the Space Shuttle Orbiter). A rigid Mid-L/D shape has advantages for large mass Mars EDL, including loads management, range capability during entry, and human spaceflight heritage. Previous large mass Mars studies have focused more on symmetric and/or circular cross-section Mid-L/D shapes such as the ellipsoid. More recent work has shown performance advantages for non-circular cross section shapes. This paper will describe efforts to design a rigid Mid-L/D entry vehicle for Mars which shows mass and performance improvements over previous Mid-L/D studies. The proposed concept, work to date and evolution, forward path, and suggested future strategy are described.

Nomenclature

C_L	= aerodynamic coefficient of lift
C_D	= aerodynamic coefficient of drag
g	= acceleration due to gravity
L/D	= lift-to-drag ratio
q	= heat flux, W/cm ²
ρ_∞	= freestream density, kg/m ³

¹ Chief, Flight Mechanics and Trajectory Design Branch, NASA JSC/EG5, AIAA Senior Member.

² Precision Landing and Hazard Avoidance Domain Lead, Flight Mechanics and Trajectory Design Branch, NASA JSC/EG5.

³ Aerospace Engineer, Flight Mechanics and Trajectory Design Branch, NASA JSC/EG5, AIAA Senior Member.

⁴ Project Manager, Project Management and Integration Office, NASA JSC/EA5.

⁵ Aerospace Engineer, Applied Aeroscience and CFD Branch, NASA JSC/EG3.

⁶ Aerospace Engineer, Flight Mechanics and Trajectory Design Branch, NASA JSC/EG5, AIAA Senior Member.

⁷ Aerospace Engineer, Flight Mechanics and Trajectory Design Branch, NASA JSC/EG5.

⁸ Aerospace Engineer, Flight Mechanics and Trajectory Design Branch, NASA JSC/EG5.

⁹ Aerospace Engineer, Systems Analysis Office, Aeronautics Directorate, NASA ARC, AIAA Senior Member.

¹⁰ Aerospace Engineer, Systems Analysis Office, Aeronautics Directorate, NASA ARC.

¹¹ Aerospace Engineer, Systems Analysis Office, Aeronautics Directorate, NASA ARC.

¹² Aerospace Engineer, Atmospheric Flight and Entry Systems Branch, NASA LaRC, AIAA Senior Member.

V_{∞}	=	freestream velocity, km/s
X_{CG}	=	x-position of the center of mass, meters
Y_{CG}	=	y-position of the center of mass, meters

I. Introduction

Humans have long been fascinated with Mars. The earliest visions of human missions to Mars come from science fiction and involved a wide range of methods of transportation¹. In his publication *Das Marsprojekt*, Wernher von Braun outlined an early technical approach to a human Mars mission campaign². Von Braun's approach utilized a winged landing craft, but at the time the low density of the Martian atmosphere was unknown. More recent studies have considered multiple approaches for large mass Mars landing, a number of which merit continued study. One of the approaches which has shown merit has become known as "Mid-L/D", used to describe an entry vehicle which is flown at a hypersonic lift-to-drag ratio between that of a typical entry capsule ($L/D \sim 0.3$) and that of the Space Shuttle Orbiter ($L/D \sim 1.5$) or higher L/D winged vehicles. The Mid-L/D vehicle is intended to be flown at $L/D = 0.5$ - 0.7 hypersonically and supersonically.

In the 1990s, a study considered a rigid Mid-L/D approach coined as the "ellipsled" as part of an effort to perform aerobraking/aerocapture for a habitation module called TransHab³. The ellipsled was desirable since it was roughly the shape of a payload fairing (PLF) of a launch vehicle. It was thought that the launch vehicle PLF could double as the aero-entry "aerobrake" for atmospheric maneuvers. Some compromise regarding the aerodynamic shape and its performance would need to be made to best meet both ascent and aerocapture/entry requirements and the ellipsled with its circular cross-section and elliptical nose was the proposed solution. Hollis looked at variations of the geometry and worked to characterize the aerodynamics and aeroheating⁴. The ellipsled was also considered as part of additional human Mars studies.^{5,6,7} In these studies, the ellipsled aeroshell was jettisoned as needed depending on the mission phase and application. For example, the aeroshell could be jettisoned prior to landing to expose a set of engines. Aeroshell jettison prior to the supersonic retropropulsion (SRP) event was believed to reduce overall system mass, although the details of the jettison event were not studied in depth.

More recent efforts have ensued as a part of NASA's Evolvable Mars Campaign (EMC)⁸. Initially, a Cycle 0 Mid-L/D effort was completed which considered different concepts: rigid, folded wing, and deployable Rogallo wing. A rigid, slender body shape was carried forward into a Cycle 1 Design Study and is the focus of this paper.

The Mid-L/D concept continues to warrant additional design work due to the qualities and performance it can provide. The moderate lift-to-drag ratio can assist with management of loads and improve downrange and crossrange capability, as well as entry corridor width and potentially landing accuracy. A fully rigid concept reduces design, development, test, and evaluation (DDT&E) cost, leveraging proven tools, materials, control approaches, and design/verification processes. Based on existing systems and practices, it minimizes requirements for technology developments and flight testing.

The current configuration of the Mid-L/D vehicle used in the Cycle 1 Design Study embodies some of the lessons learned from the Cycle 0 analyses. Rather than serve as both the Space Launch System (SLS) launch shroud and entry/aerocapture aeroshell, it was decided to launch the Mid-L/D within the planned 10 meter (m) diameter SLS PLF. The rationale was twofold: 1) the previous dual-use approach resulted in negligible mass savings, in particular due to the necessity for acoustic blankets within the Mid-L/D shape if used as the launch rocket fairing, and 2) the impacts to the design and testing of the SLS would be significant. Thus the current Mid-L/D design efficiently utilizes the internal dimensions of the SLS PLF to maximize payload volume and aerodynamic surface area. Another finding from Cycle 0 was that deployment of a lander from within the aeroshell (i.e. aeroshell jettison) at supersonic conditions was indeed a difficult design approach which would warrant a significant flight test program. In addition, it would produce large debris on the approach to a Mars landing. In terms of overall entry mass, utilizing a deployable lander did not appear to generate much, if any, savings when including the additional mass of an aeroshell separation system. The Cycle 1 vehicle is designed with lander components integrated into the rigid aeroshell and the aeroshell is retained through landing. Supersonic retropropulsion is the only remaining major dynamic EDL event.

II. CobraMRV Mid-L/D Concept

A. Objectives

The primary objectives of the study were to design and analyze a rigid Mid-L/D vehicle concept capable of delivering 20 metric tons (mt) of cargo to the surface of Mars. The design had to satisfy a number of operational requirements and constraints. The vehicle was sized to provide sufficient mass and volume capability to accommodate

the cargo defined by the EMC team. A cargo manifest reference was provided as input. Of these items, the Mars Ascent Vehicle (MAV) was determined to be the driving design case, so the majority of the team's effort was spent addressing its incorporation into the Mid-L/D design. However, the other cargo manifests were also considered.

Additional operational constraints considered include those related to the launch vehicle (SLS), in-space operations, and surface operations. These are discussed in more detail in the Concept of Operations section.

B. Overview

The CobraMRV is a high ballistic number Mid-L/D Rigid Vehicle (MRV) concept initially designed using the Co-Optimization Bluntbody Re-entry Analysis (COBRA) shape optimization process and the parametric Cobra shape class^{9,10} developed at Ames Research Center. The resultant vehicle concept is called the CobraMRV. It is a fully rigid entry vehicle concept which minimizes DDT&E by leveraging proven heritage tools, materials, controls, and processes. This also minimizes the need for technology development and flight testing. It efficiently utilizes the dimensions of the SLS PLF to maximize payload volume and aerodynamic surface area for lift and drag at high angle-of-attack. The outer mold line (OML) is designed to provide desirable aerodynamic characteristics in pitch, yaw, and roll, as well as generate sufficient control authority from the body flaps. The shape was also designed to attempt to keep the center of mass of the CobraMRV aligned with the centerline of the SLS when mounted within the SLS PLF.

The lander components are integrated in the rigid aeroshell and the aeroshell is retained all the way to landing. In most previous studies, the Mid-L/D aeroshell was shed prior to touchdown. This is a significant difference. By retaining the aeroshell, the transition to a powered retro burn is simplified. The descent engines integrate into the lower sides of the OML. They are ignited at a supersonic condition and complete the braking and terminal descent maneuvers, safely steering the vehicle to a soft landing at a horizontal orientation. The aeroshell protects the cargo from the environment during the entry, SRP phase, and landing, as well as aerocapture. The control scheme uses reaction control system (RCS) jets for maneuvering. Split body flaps are used for trim during the aerocapture/entry phase, and main engine throttling is used for trim during the powered descent phase.

Figure 1 shows the final OML, CobraMRV 2908b, that was down selected from the Pareto front of optimized shapes obtained through the COBRA shape optimization process. The vehicle is 19.8 m long by 8.8 m wide at the maximum width point. The maximum height point occurs at the aft most portion of the vehicle and is 7.3 m. A split body flap with an approximate 31 deg cant is placed aft of the vehicle with a fairing along the aft lower surface to accomplish a smooth transition from the windside base shape to the actuating rectangular body flaps which are 1.6 m long by 4 m wide, as shown in Fig. 1. As a point of comparison, the total flap area is very similar to that of the Space Shuttle Orbiter body flap (12.62 m²). Doors on top of the vehicle allow access to the interior cargo bay, similar to the Space Shuttle payload bay doors, and the rear incorporates a door which rotates down to become an access ramp when deployed.

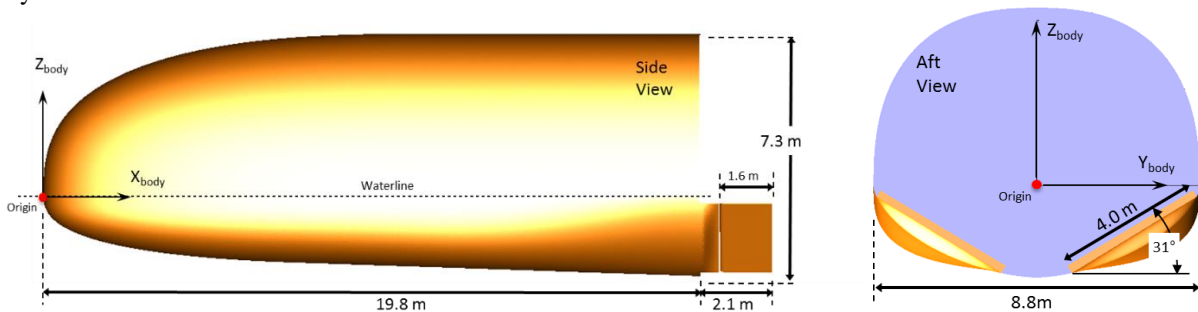


Figure 1. Outer Mold Line definition (CobraMRV 2908b).

C. Concept of Operations

The CobraMRV developed to support the EMC architecture is launched on a SLS Block 2 Launch Vehicle within a 10 m PLF. Figure 2**Error! Reference source not found.** shows the CobraMRV in the launch configuration with an external Solar Electric Propulsion (SEP) stage mounted within a representative payload adapter. The CobraMRV maximizes the use of the available PLF dimensions and the estimated center of gravity of the vehicle stack is located on the SLS centerline. Following the launch of the CobraMRV into a transfer orbit, the SEP stage is used to initiate a gradual outward spiral into a trans-Mars trajectory. Spiral time to Earth escape for a reference 300 kW SEP is approximately 2.5 years.

During the Earth to Mars Transit phase, the CobraMRV relies on the SEP stage for propulsion, power and communications. Thermal control for the CobraMRV is provided via deployable radiators mounted on the inner surfaces of the cargo bay doors, similar to the Space Shuttle. The transit time between Earth and Mars for the assumed reference trajectory is 1.2 years. The SLS

injection orbit and the durations of the outward spiral and Mars transit are driven by the gross mass of the CobraMRV.

Two days prior to arrival at Mars, the SEP stage is jettisoned and the CobraMRV assumes responsibility for power generation and communications. Fuel cells utilize the liquid methane and oxygen propellants stored in the CobraMRV descent and landing tanks to generate electrical power. Since the cargo bay doors must be closed for the aerocapture maneuver, a water sublimation system is used to reject waste heat until the radiators can be redeployed. Following the completion of successful capture at Mars, the CobraMRV RCS is used to enter the reference orbit.

For EMC cargo delivery missions, the CobraMRV will typically stay in Mars orbit for only a short period of time before initiating the de-orbit maneuver. For a crewed mission, however, the CobraMRV may need to remain in Mars orbit for up to a year before the crew arrives in a separate transit vehicle. During this extended parking orbit, a set of solar arrays is deployed to generate electrical power. After the crew transfers into the CobraMRV and completes the vehicle checkout, the solar arrays are jettisoned and the cargo bay doors are closed to prepare for de-orbit followed by entry, descent, and landing (EDL). With the exception of minor differences in vehicle mass properties due to consumables and jettisoned hardware, the aerocapture and entry configurations of the CobraMRV are identical.

To initiate the EDL sequence, a de-orbit burn is completed using the RCS. The vehicle performs a lifting entry, using RCS bank angle modulation to manage g-loads and steer the vehicle accurately to the landing target. Split body flaps are used to provide pitch and yaw trim across the Mach range. As the vehicle approaches the surface of Mars, panels on either side of the windward heat shield are either articulated or jettisoned to expose two banks of descent main engines. The engines are ignited at supersonic free stream conditions and are used to decelerate the

CobraMRV to a soft, controlled landing. Figure 3**Error! Reference source not found.**

Figure 3. CobraMRV Entry, Descent, and Landing. illustrates the nominal entry, descent, and landing (EDL) sequence.

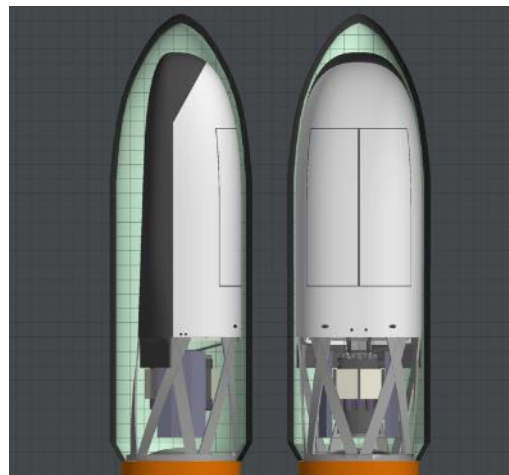


Figure 2. CobraMRV in SLS 10 m PLF.

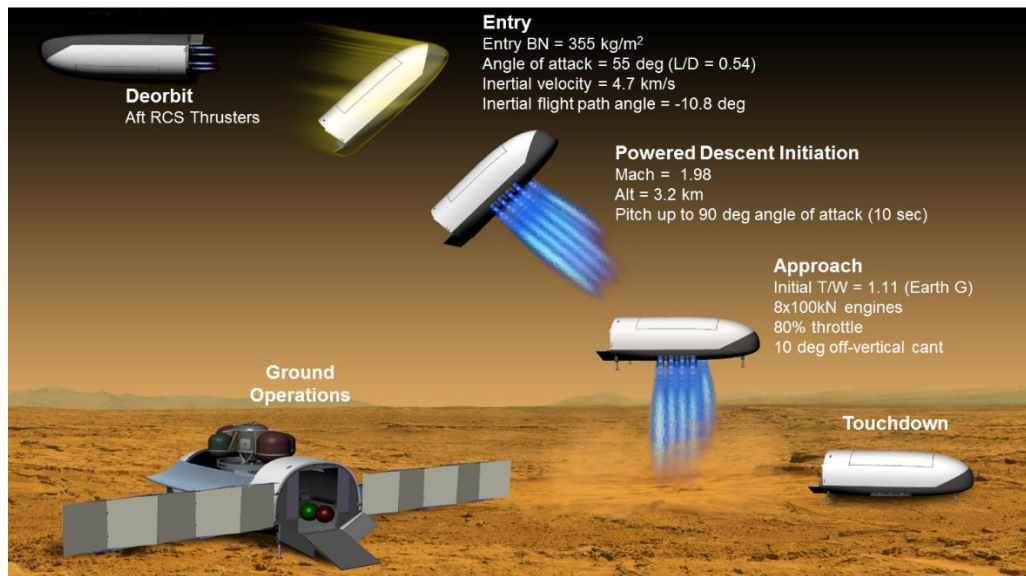


Figure 3. CobraMRV Entry, Descent, and Landing.

The transition to powered descent at Mars occurs at a relatively low altitude and high velocity, as noted in Figure 3. The delta-V allocation for the Mars powered descent maneuver is 650 m/s – roughly one-third of the delta-V required for powered descent at the Moon – and the retained aeroshell continues to contribute some drag. As a result of these factors, the mass impact of retaining the aeroshell through landing is not as large as might be expected. The aeroshell also protects the lander systems and cargo from the SRP flowfield, as well as the ejecta and dust generated during terminal descent and landing. In addition, the elimination of aeroshell disposal constraints for emplaced surface assets provides greater flexibility in the design and optimization of the Mars EDL trajectory.

Surface operations begin after the vehicle has landed safely on Mars. Using the residual methane and oxygen propellants from the CobraMRV descent tanks, fuel cells provide electrical power for up to 24 hours until the connection to a surface power system is established. Two radiator panels stowed on the aft of the CobraMRV are deployed to provide thermal control for the vehicle systems and cargo on the surface of Mars. As shown in Figure 3, very large radiators are required to support the generation and liquefaction of oxygen from the atmosphere of Mars to fill the MAV tanks. The primary function of the cargo bay doors is to enable a vertical launch of the MAV from the landed CobraMRV. The cargo bay door radiators are not required on the surface of Mars, so the cargo bay doors can be opened or remain closed, as appropriate for each cargo configuration. In addition, a ramp can be deployed from the aft end of the vehicle, as shown in Figure 4, to **Error! Reference source not found.** provide flexible and convenient access to the internal cargo bay for mobile vehicles and personnel. The ramp can also be stowed to provide protection from dust storms.

The CobraMRV team developed several operational scenarios for launching the MAV. In the reference approach illustrated in Figure 4, the MAV crew approaches the CobraMRV in a pressurized rover (1) and executes an intra-vehicular (IVA) transfer to the MAV crew module (2). Following a successful MAV checkout, the rover departs and the transfer tunnel is retracted (3). The cargo bay doors are then opened to enable the launch of the MAV (4). To help alleviate concerns regarding the vibro-acoustic environment at liftoff, the MAV is mechanically elevated several meters with a flame deflector directing the engine exhaust out the aft end of the vehicle (5). The MAV then begins its ascent to Mars orbit (6). During the design process, it became clear that the cargo bay doors imposed a significant mass penalty on the vehicle primary structure. As a result, the CobraMRV team outlined several scenarios involving the aft extraction of the MAV from the CobraMRV aeroshell via a rail system or a wheeled cart, for future consideration. The 2908b variant of the CobraMRV aeroshell and the interior subsystem layout illustrated in Figure 4 and Figure 5 are intended to facilitate the aft insertion/extraction of large cargo items.

MAV Launch Operations from CobraMRV

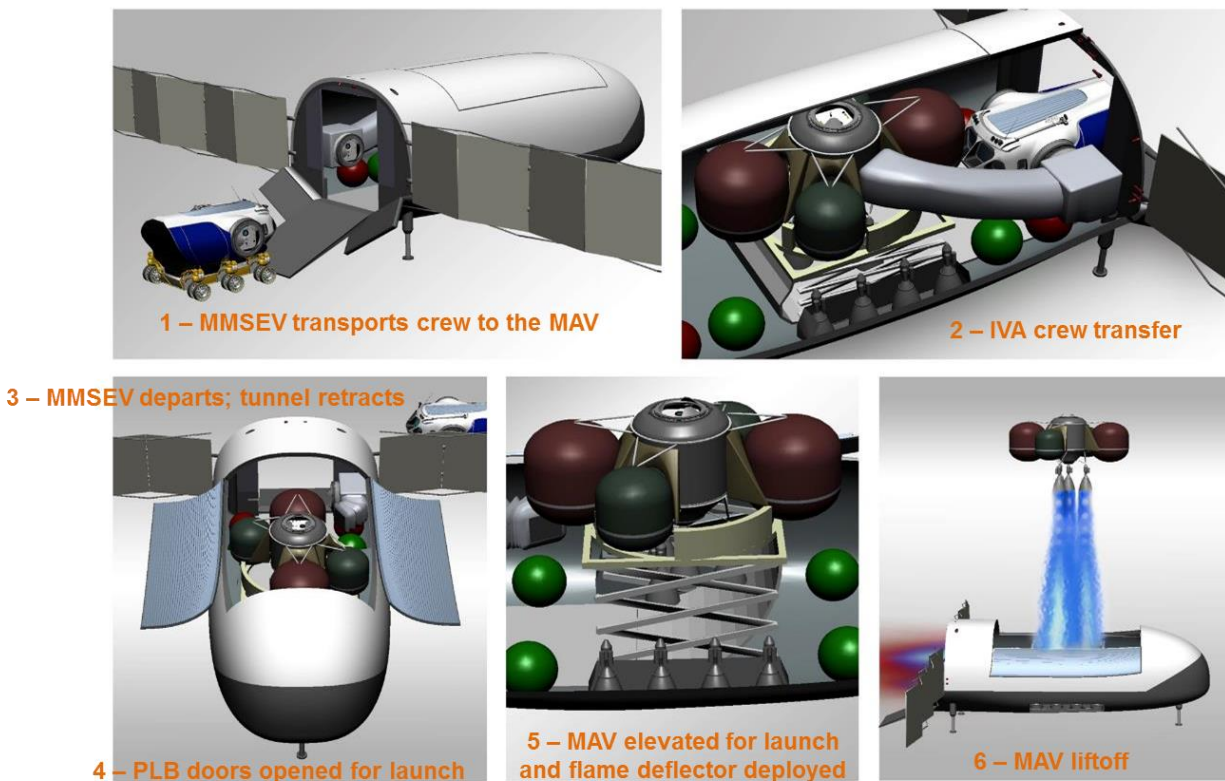


Figure 4. Concept of Operations for MAV Launch.

D. Vehicle Integration and Structural Design

The CobraMRV rigid body is an efficient and flexible EDL platform for the delivery of cargo to the surface of Mars. The aeroshell configuration reflects a balance between the mass, volume, and operational requirements for the EMC reference cargo configurations and key EDL performance requirements, including aerodynamic and stability and control characteristics. In addition to EDL and Mars surface operations, the CobraMRV, as an element of a large and complex Mars transportation architecture, must also reflect end-to-end life cycle considerations, such as manufacturing and assembly, testing, flight certification, ground processing, launch vehicle integration, launch operations, and in-space operations.

The “truck-like” CobraMRV fuselage supports a comprehensive Mars surface mobility strategy. The 4.0 m wide aft access ramp combined with the low 2.1 m cargo deck height enables the efficient utilization of rovers, carts, and other mobile units in a multiple lander mission architecture with landing sites spread across several square kilometers. These CobraMRV design features also simplify IVA crew and cargo transfers with surface transportation elements and enable efficient EVA crew access to the surface of Mars using the aft ramp or a short set of stairs.

The interior layout of the CobraMRV aeroshell is driven by the EMC requirement for a large, general purpose cargo bay. The cargo bay is centralized to anchor the vehicle center of gravity near the reference aerodynamic trim point. The arrangement of the vehicle subsystems, particularly the propulsion system elements, about the central cargo area is designed to maximize the available cargo volume/dimensions, as well as to provide a wide central corridor to support a variety of cargo elements – MAV, surface habitat, logistics modules, rovers, racks, and containers.

The MAV is the most challenging of the EMC cargo elements. It is a large and massive spacecraft that must be loaded with liquid methane prior to SLS launch, maintained in a zero boil-off state throughout the mission, and gradually filled with liquid oxygen that is generated from the atmosphere of Mars via an in-situ resource utilization (ISRU) system post-landing. At the end of the surface mission, all of the external mechanical, fluid, data, and power connections between the CobraMRV and the MAV must be severed to enable MAV liftoff. It should be noted that the MAV shown in **Error! Reference source not found.** and Figure 5 was originally developed for the HIAD concept, a blunt body decelerator with a circular rigid heat shield augmented with inflatable toroids to increase drag area. A

redesign of the MAV tailored for the CobraMRV will improve load path integration with the CobraMRV aeroshell primary structure for launch and entry. The MAV side hatch would also be clocked aft to eliminate the necessity for a rover docking tunnel and to simplify IVA crew and cargo transfer.

The propulsion system consists of eight descent engines arranged in two banks of four. Each LO₂/LCH₄ engine provides a maximum thrust of 100 kN, for a total of 800 kN. The engines are located to either side of the cargo bay with an outward cant angle of 10 degrees. The location and orientation of the engines is designed to nominally provide a balanced moment state during powered flight with differential main engine throttling used for gross pitch and roll control. The propulsion system also includes twenty RCS thrusters providing 4,450 N each, which are used for active flight control and attitude maintenance during atmospheric and powered flight. This includes a set of four axial RCS thrusters which are used for small orbit adjust maneuvers, including the de-orbit burn. Four pairs of spherical propellant tanks are arranged symmetrically fore and aft of the main cargo area to limit center of gravity migration during powered flight.

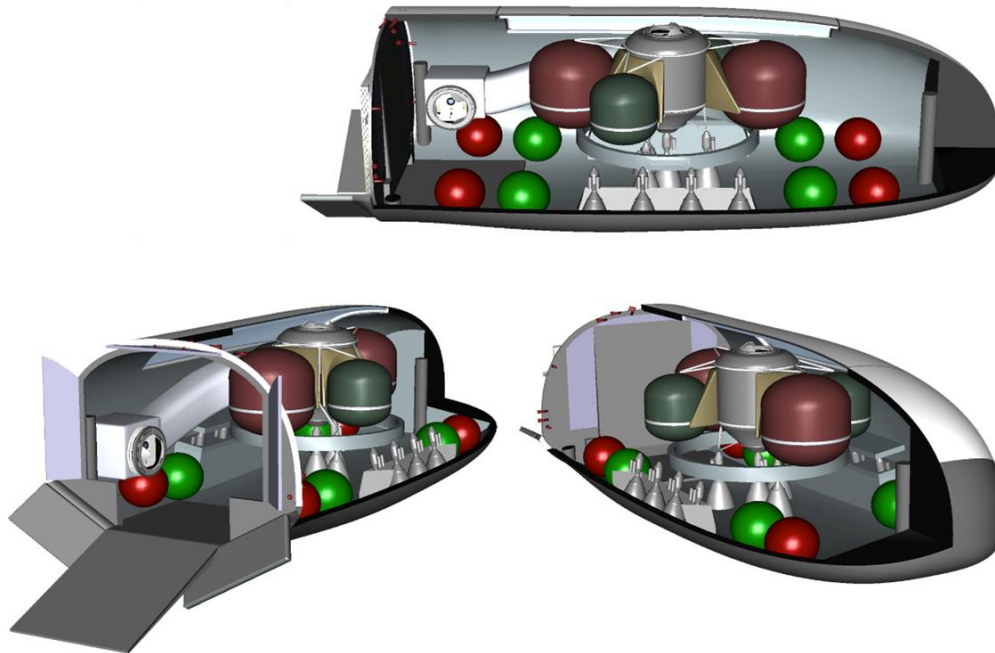


Figure 5. Cutaway View of CobraMRV.

One of the key advantages of the CobraMRV concept is the extensive aerospace heritage in the design, analysis, manufacturing, testing, and certification of rigid entry bodies. The CobraMRV team combined expertise and analysis tools from several NASA centers to evaluate structural layouts and key design features at varying levels of detail to gain an improved understanding of the structural sensitivities and mass drivers. The resulting CobraMRV preliminary structural design is based on a traditional semi-monocoque approach combining a stressed skin and a primary structure composed of longerons, ribs, and frames. The cargo bay doors were conservatively modeled as non-load bearing elements. Conventional aluminum alloys were utilized for the primary and secondary structure and skin panels to reduce overall DDT&E cost and risk. To support the initial structural layout and mass estimation process, enveloping load cases were developed for Earth launch (5.0 g axial, 2.0 g transverse) and entry, propulsive deceleration, and landing at Mars. Entry loads were based on EDL trajectory simulations, with the trajectories constrained to avoid exceeding 4.0 g through the chest for the crew for any substantial duration.

E. Flight Performance

1. Aerodynamics and Stability

The aerodynamics for the CobraMRV 2908b configuration were calculated using the Cart3d Euler CFD code for a Mach range of 1.5 – 12. **Error! Reference source not found.** shows the lift coefficient, drag coefficient, and L/D. The coefficients shown were calculated for a reference area of 65 m², with an associated reference length of 9.1 m. During hypersonic entry, the vehicle is trimmed at an angle of attack of 55 deg. This results in an L/D of 0.54, with an associated trim center of gravity (CG) location 10.55 m back from the nose and 1 m above the waterline.

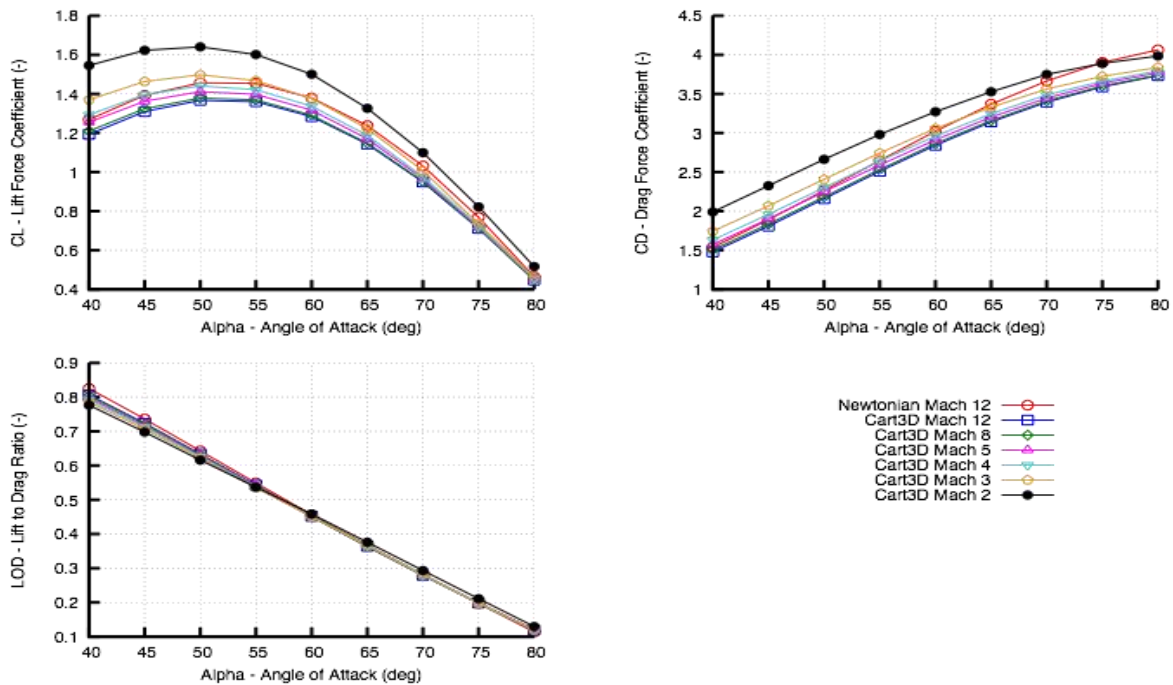


Figure 6. Aerodynamic Coefficients for CobraMRV 2908b with Reference Area = 65 m².

A split flap is used during entry to help maintain the desired angle of attack and to minimize the sideslip angle, as shown in Figure 7. CobraMRV split flap at 15 deg and 20 deg deflection. **Error! Reference source not found.** The flaps were sized to provide a sufficient trim capability for a range of CG locations, based on Shuttle orbiter experience. Angle of attack trim sensitivity, without flap (elevon) deflections, to changes in X_{CG} (fore/aft), is 0.38 deg/cm. However, by utilizing elevon deflections, the X_{CG} capability is sized to +/- 20 cm while still maintaining a 55 deg trim angle of attack across the full Mach regime from supersonic to hypersonic. This range of X_{CG} capability is the same percentage of the body length as the Shuttle orbiter. Using minimal aileron deflections and sideslip angles, the Y_{CG} capability allows for up to +/-5 cm deviation, which is three times the off-centerline capability of the Shuttle orbiter. These values are for elevon deflections of +/-20 deg and +/-2.5 deg aileron deflection.

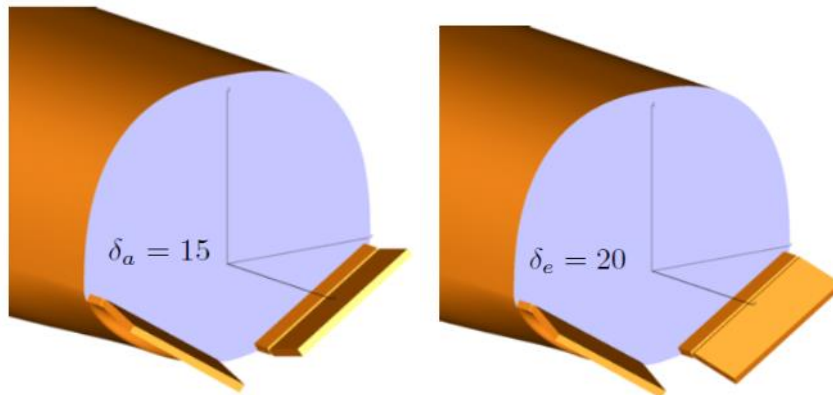


Figure 7. CobraMRV split flap at 15 deg and 20 deg deflection.

During the powered descent portion of flight, differential throttle is used to perform trim management of the vehicle.

Primary attitude maneuvering throughout all atmospheric phases is accomplished via a set of 20 x 4,450 N (1,000 lb) RCS jets. The jets are all notionally located in the aft plane of the vehicle, and are sized to provide a minimum of 5 deg/sec² of torque in the roll, pitch, and yaw body axes.

2. Aerocapture Trajectory

The vehicle arrives at Mars with a relative velocity of 6.2 km/s (study assumption). The post-aerocapture target orbit at Mars has a period of 1 sol (250 km by 33,793 km). The purpose of aerocapture is to reduce the spacecraft energy to the target 1 sol orbit using a single atmospheric braking maneuver.

Following the aerocapture, a two burn sequence is assumed to achieve the final orbit. The first burn occurs at apoapsis, and is used to raise the periapsis to the 250 km altitude. Without this maneuver, the spacecraft would re-enter the atmosphere. The second of the two burns is a cleanup maneuver (nominally zero delta-V) to adjust the apoapsis to the final target of 33,793 km.

The nominal aerocapture trajectory is shown in Figure 8. The aerocapture trajectory assessment was performed using the Flight Analysis Simulation Tool (FAST). The left panel shows the altitude vs velocity profile. The spacecraft enters at 6.2 km/s and exits at about 4.7 km/s. The plot shows a minimum altitude of 40 km during aerocapture. The right panel depicts the sensed acceleration, in Earth g. The nominal case shows a peak g-load of 1.3 Earth g. The aerocapture trajectory was used as input to determine the set of flight conditions for aerothermal cases.

A Monte Carlo assessment was also completed for aerocapture¹¹. As a result of this assessment, the delta-V budget for post-aerocapture cleanup was determined to be 40 m/s.

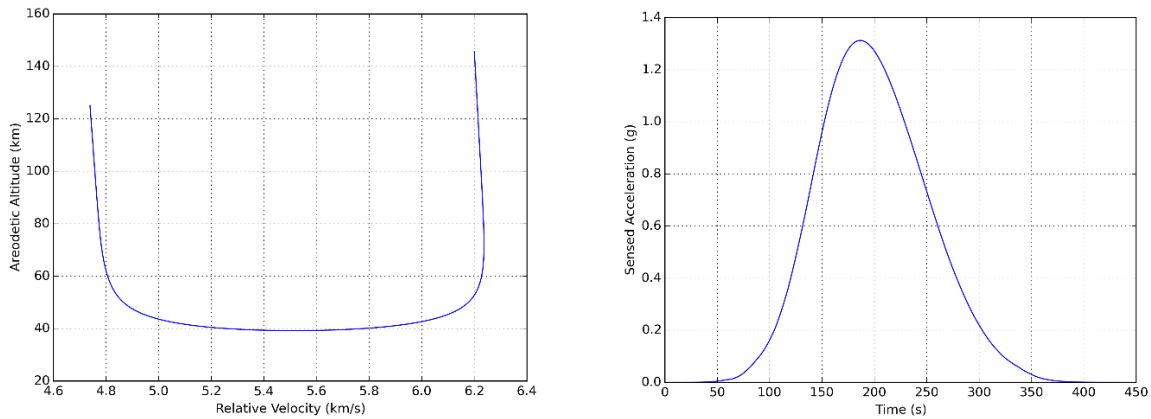


Figure 8. Nominal Aerocapture Trajectory.

3. Entry, Descent, and Landing Trajectory

Following a period of loiter in Mars orbit, a de-orbit burn is performed to target the desired Entry Interface (EI) state. The in-plane nominal delta-V for this burn is 17 m/s. A total of 20 m/s was budgeted for this maneuver, based on engineering assumptions.

The simulation used for the EDL analysis is the Simulation of Rocket Trajectories (SORT) tool¹². Table 1 shows the assumed entry state and key assumptions used in the EDL simulation. The inertial flight path angle of -10.8 deg was selected during the design process. The rest of the variables in the table are assumptions. The Mars GRAM 2005 atmospheric model was used, with an epoch of May 10, 2033, 0:00 UTC.

Table 1. Entry State and Key EDL Assumptions.

Parameter	Value	Units
Geocentric radius	3522200	m
Declination	81.558	deg
Longitude	0.0	deg
Inertial Velocity	4700	m/s
Inertial Azimuth	180	deg
Inertial Flight path angle	-10.8	deg
Total main engine thrust	8*100,000	N
Main engine cant angle	10.0	deg

Main engine Isp	360	sec
RCS Isp	325	sec

The entry bank profile is selected using parameter optimization. The optimizer is given eight bank segments to determine a bank profile which minimizes Mach number at a given altitude for the start of SRP. Limits are placed on the range of bank angle that can be selected. A range of 10 deg (near full lift-up) to 90 deg (lift vector to the side) of bank angle was used for this study. Additionally, a minimum altitude constraint and a limit on the maximum vertical velocity are used to ensure that the solution will have sufficient margin for guided, dispersed cases. Figure 9 shows the nominal bank profile. At 1000 m/s relative velocity, a 10 deg bank angle is held until the start of the powered flight phase.

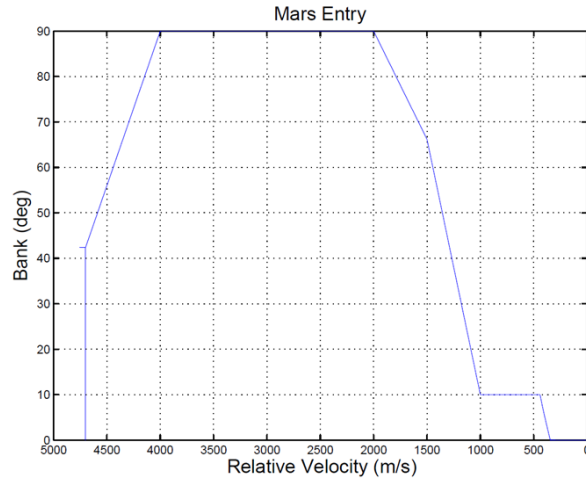


Figure 9. Nominal Entry Bank Profile.

The resulting nominal trajectory is shown in Figure. The maximum dynamic pressure is 7700 Pa. The maximum load is limited to 2.5 g, and occurs at the same velocity as the maximum dynamic pressure, approximately 3400 m/s. The magnitude of the load pulse is shown in the right panel of Figure 10. The entry load ramps up at 100 sec after EI, and continues for just over six minutes for this trajectory, dropping to 0.4 g during the lift-up portion near the end of the entry phrase. The powered descent burn begins at about 480 sec post-EI at a Mach number of just under Mach 2. For the constant thrust portion of the burn, the loads vary from about 1.1-1.3 Earth g (at 80% throttle). A constant velocity phase of 1.0 Mars g (0.38 Earth g) begins at 12.5 m above the surface, with an assumed touchdown velocity of 2.5 m/s. (not shown in Figure.)

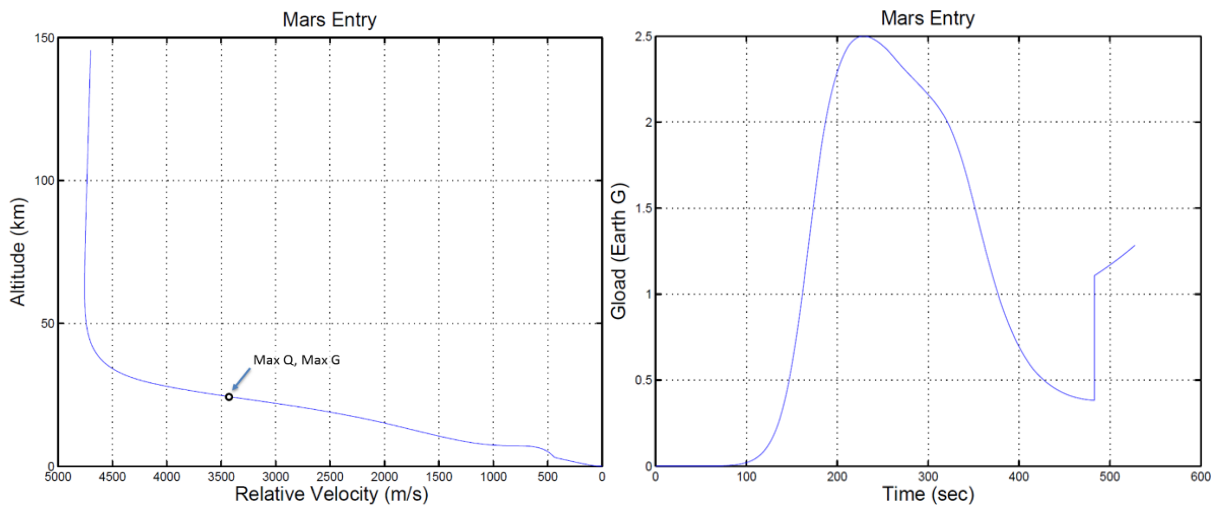


Figure 10. Nominal EDL Trajectory.

The selection of the altitude to transition to powered descent, or SRP phase, is a crucial performance variable. The SRP maneuver should begin at a sufficiently high altitude for the powered descent to be able to remove any remaining velocity following aerodynamic entry, as well as fly out any state error. The lowest altitude that enables the elimination of these errors, given maximum thrust limits, will likely provide the minimum propellant solution. During Cycle 1, the selected nominal transition altitude was just under 3.2 km. Figure 11 shows that for every kilometer increase in altitude, an additional 600 kg of propellant is required. Monte Carlo analysis will drive the selection of this transition altitude parameter. Preliminary Monte Carlo analysis for the entry, descent, and landing has been completed using the FNPEG¹³ guidance algorithm and is planned as the subject of a future paper.

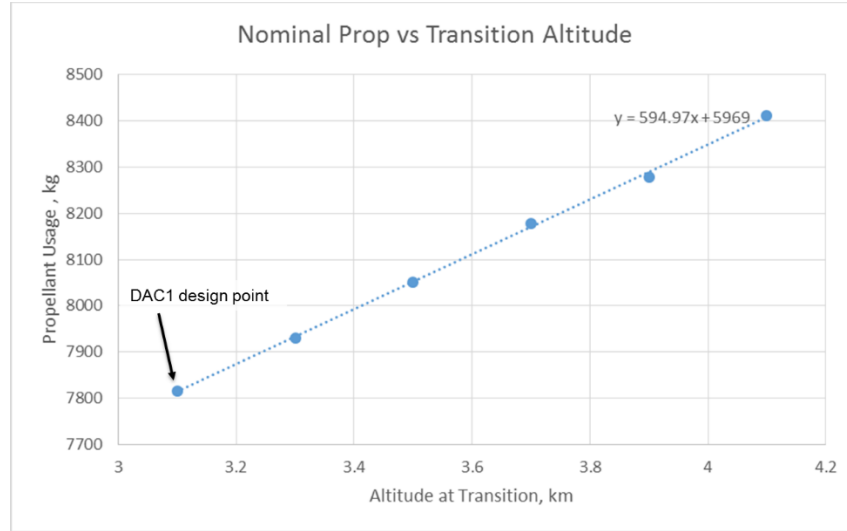


Figure 11. Transition to SRP Sensitivity.

F. Aerothermal

High-fidelity predictions of aerothermal environments were made using the Langley Aerothermodynamic Upwind Relaxation Algorithm (LAURA) code^{14,15} and the High-Temperature Aerothermodynamic Radiation (HARA) code^{16,17}, which provided convective and radiative heat flux distributions, respectively. Freestream composition was assumed to be 97% CO₂ and 3% N₂ by mass while the flowfield was modeled with an eight-species composition: CO₂, CO, N₂, O₂, NO, C, N, and O. The vehicle surface was modeled as fully-catalytic to homogeneous recombination and having a radiative equilibrium temperature. In the present study, the HARA radiative heat flux calculations were performed on fully-converged LAURA flowfield calculations using the tangent-slab approach.

Freestream conditions for these CFD calculations were taken at points spaced out along the aerocapture and entry trajectories so as to bound the heat pulses. The trimmed vehicle attitude of 55 degrees angle of attack was applied to all cases. Based upon an assessment of the laminar solutions (particularly the ratio of laminar momentum-thickness Reynolds number to boundary-layer edge Mach number), transition to turbulence was predicted to occur early in the trajectory, prior to peak heating. Therefore, fully-turbulent convective heat flux predictions were made for all database solutions, using the Cebeci-Smith algebraic turbulence model¹⁸. Additionally, only windward distributions were provided for database development. Accurate leeside predictions of convective heat flux require more computationally-complex turbulence models and higher-resolution grids to accurately capture the separated wake flow. Accurate leeside modeling of radiative heat flux would further require the volume grid to be extended into the base flow region to enable application of a full ray-tracing approach¹⁹, rather than the less computationally-demanding tangent-slab approach.

A complete database of high-fidelity solutions was developed for the CobraMRV based upon an initial configuration of the vehicle (CobraMRV 7212a). This database was then used to anchor engineering-fidelity aerothermal models used for vehicle TPS sizing. Continued iterative improvements to the CobraMRV design eventually led to an updated configuration (CobraMRV 2908b). An attempt was made to leverage the existing CobraMRV 7212a database of CFD solutions such that a small number of additional CFD solutions applied to CobraMRV 2908b could be used to generate correction factors for the existing CobraMRV 7212a engineering aerothermal models. To this end, four freestream conditions were identified for analysis of the CobraMRV 2908b

configuration. These were the freestream conditions corresponding to CobraMRV 7212a peak convective and peak radiative heat flux along both the aerocapture and entry trajectories.

To illustrate the aerothermal environments predicted for the CobraMRV, Figure 12 and Figure 13 show unmargined high-fidelity CFD heat flux distributions for the 2908b configuration. This solution corresponds to the freestream condition at which maximum total heat flux is encountered during aerocapture. Figure 12 depicts total laminar and turbulent heat flux distributions along the vehicle windward centerline, along with a breakdown into convective and radiative components. A contour plot of total turbulent heat flux along the entire windward surface is provided in Figure 13. With the contribution of radiation, the total heat flux is largest at the aft end of the body, reaching a value of approximately 55 W/cm². Overall, the heating is high in both the forward nose region and at the aft end of the vehicle.

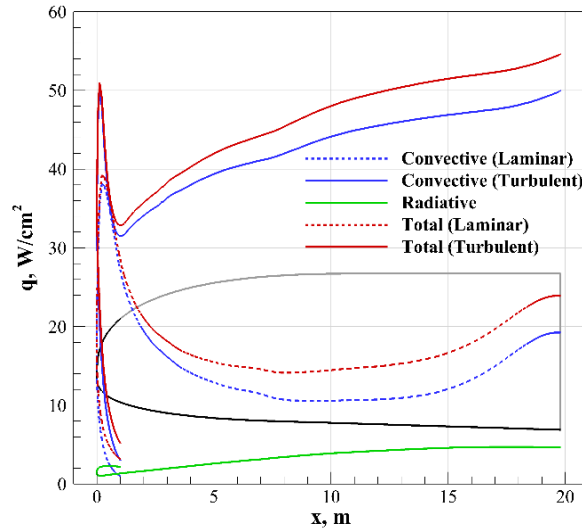


Figure 12. CobraMRV 2908b windward centerline (unmargined) heat flux distributions at the peak total heat flux conditions: $V_\infty = 5.65$ km/s and $\rho_\infty = 2.9 \times 10^{-4}$ kg/m³.

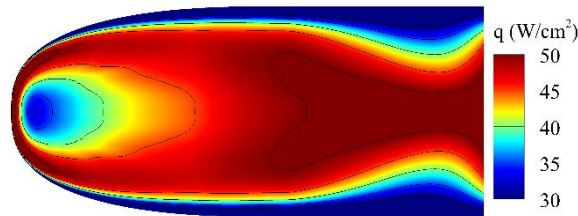


Figure 13. CobraMRV 2908b windward (unmargined) turbulent total heat flux distribution at peak total heat flux conditions: $V_\infty = 5.65$ km/s and $\rho_\infty = 2.9 \times 10^{-4}$ kg/m³.

Several trends in heat flux distribution have been identified by observing the solutions in the high-fidelity database. Peak convective heat flux generally occurs on the nose region of the vehicle as the flow rapidly expands forward away from the stagnation point and onto the leeside of the body. This peak is evident for both laminar and turbulent flows, but tends to be further augmented by turbulence. For the CobraMRV 2908b configuration, there is a milder peak in convective heat flux that occurs at the centerline of the canted aft-end of the body. Turbulence augments the convective heat flux increase in moving aft along the centerline away from the stagnation point as the boundary layer grows more rapidly and entrains higher-energy flow from within the shock layer. For the condition shown in Figure 12, this turbulent-augmented heat flux at the aft centerline of the body is on par with the peak at the nose region. The radiative heat flux was found to generally increase with distance along the body as the shock stand-off distance grew monotonically and exposed the surface to a larger volume of radiating gas.

Table 2 lists the values of unmarginized maximum total heat flux on the CobraMRV 2908b windward surface, along with the corresponding breakdown into convective and radiative components. The trajectory conditions shown correspond to peaks in convective and radiative heat flux histories along the aerocapture and entry trajectories. In terms of relative magnitude, convective heat flux is the dominant contributor to total heating compared to radiative heat flux over the entire aerocapture trajectory. The convective heat flux values experienced by the vehicle are the highest along the aerocapture trajectory. In contrast, the vehicle experiences highest radiative heat flux late along the entry trajectory. In the later portions of the entry trajectory, radiative heat flux was seen to be comparable to – or even exceed – the magnitudes of convective heat flux at the aft end of the vehicle. At these slower velocities, the CO₂ molecules experience thermal excitation as they pass through the bow shock, but the resulting temperatures are not high enough for dissociation to occur. Rather, these excited molecules emit infrared radiation, contributing significantly to the total incident heat flux to the vehicle surface. Thus, the radiative heat flux component cannot be neglected, even for entry from orbit, in making accurate predictions of total heat load at Mars.

Table 2. CobraMRV-2908b Maximum (Unmarginized) Total Heat Flux along Aerocapture and Entry Trajectories at Conditions Corresponding to Peak Convective and Radiative Heat Flux.

	Aerocapture		Entry	
	Peak Convective Condition	Peak Radiative Condition	Peak Convective Condition	Peak Radiative Condition
V_{∞} , km/s	5.65	5.10	4.34	3.05
ρ_{∞} , kg/m ³	2.90×10^{-4}	3.14×10^{-4}	7.19×10^{-4}	1.65×10^{-3}
$q_{total} (q_{conv} + q_{rad})$, W/cm ²	55.0 (54.0+1.0) ⁿ	38.5 (32.2+6.3) ^a	38.0 (27.3+10.7) ^a	26.3 (12.9+13.4) ^a

Note: Superscript **n** denotes that maximum heat flux occurs in the nose region; **a** denotes that it occurs in the aft region.

G. Thermal Protection System

Preliminary TPS materials selection and TPS sizing was performed based on the provided aeroheating environments and trajectories. The solutions were obtained by extrapolating from the provided inputs, and employing CFD-anchored aerothermal databases based on the CBAERO software²⁰. TPS material selection criteria were based on expected heating environments with margins. The TPSSizer software²¹ is used to perform the design. The TPS design employs a rigid outer aeroshell with the TPS bonded to the structure. Dual heat pulse capability is required for the Mid-L/D TPS materials. Two OML configurations were investigated, starting initially with the CobraMRV 7212a shape, and then transitioning to the CobraMRV 2908b configuration for improved performance.

The aerocapture and entry time histories are concatenated into a single continuous trajectory, and the aeroheating environments are then obtained as a function of time along the aerocapture and entry trajectory by interpolating the aerothermal data base as a function of Mach number, freestream dynamic pressure and angle of attack. For the heat transfer analysis, as part of the TPS sizing process, a sufficiently long in-orbit cool off period is inserted at the end of the aerocapture trajectory and the beginning of the entry trajectory.

Mission maximum surface temperature distribution is shown in **Error! Reference source not found.4**, which is used as the basis for the TPS material selection. Several candidate windward TPS materials were evaluated, including TUF_I coated AETB-8 tile and other ablator systems (SLA-561V and Conformal PICA). **Error! Reference source not found.** summarizes the TPS system masses for the various candidate materials. The margined maximum surface temperatures observed are above the allowable limit for reusable TPS materials (e.g. TUF_I coated tile). Body flaps are assumed to be hot structure and no TPS estimate was provided for the body flap TPS.

The selected windward TPS consists of Lightweight Ceramic Ablators (LCA) consisting of rigid silica tiles with infused silicone (specifically the Silicone Impregnated Rigid Ceramic Ablator, SIRCA-15), and Shuttle-derived flexible blankets (AFRSI and FRSI) were selected for the leeward surfaces. Figure 155 presents the windward and leeward candidate TPS materials and their associated stack-ups. The leeward TPS consists of Shuttle heritage flexible blankets FRSI and AFRSI. The corresponding TPS material split lines are presented in **Error! Reference source not found.6**. For the range of heating rates seen, the thermal response of SIRCA is limited to pyrolysis of the injected silicone, with no associated surface recession. Figure 17 presents the TPS material thickness distribution for the selected baseline TPS material selection (SIRCA-15, AFRSI & FRSI), and the resulting TPS areal mass is shown in Figure 178. Maximum SIRCA-15 thickness is approximately 5 cm, with both the FRSI and AFRSI at or near minimum gauge thickness, approximately 0.64 cm (0.25 inches). Further development efforts for dual-use TPS

materials should be pursued. Dual-use, mass efficient materials in the 100 W/cm² range are particularly needed for the Mid-L/D configuration.

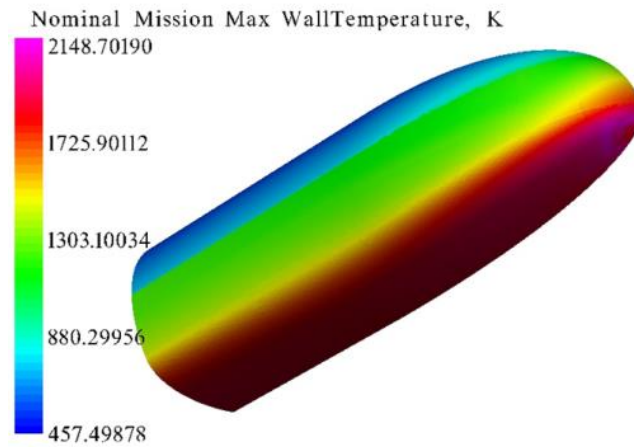


Figure 144. Mission Max Temperatures.

Table 3. TPS System Mass for Candidate Materials.

Windward TPS Concept->	AETB/TUFI	AFRSI/SI	SLA-561	SIRCA	LI-2200	C-PICA	TUFROC
FRSI Mass (kg)	260	260	260	260	260	260	260
AFRSI Mass (kg)	197	197	197	197	197	197	197
Windward TPS Areal Density (kg/m ²)	9.3	8.6	7.2	10.6	15.0	11.9	17.4
Windward TPS Mass (kg)	1801	1676	1401	2070	2915	2318	3378
Total TPS Mass (kg)	2258	2132	1857	2527	3371	2774	3835
Dry Mass Fraction	8.7%	8.2%	7.1%	9.7%	12.9%	10.7%	14.7%

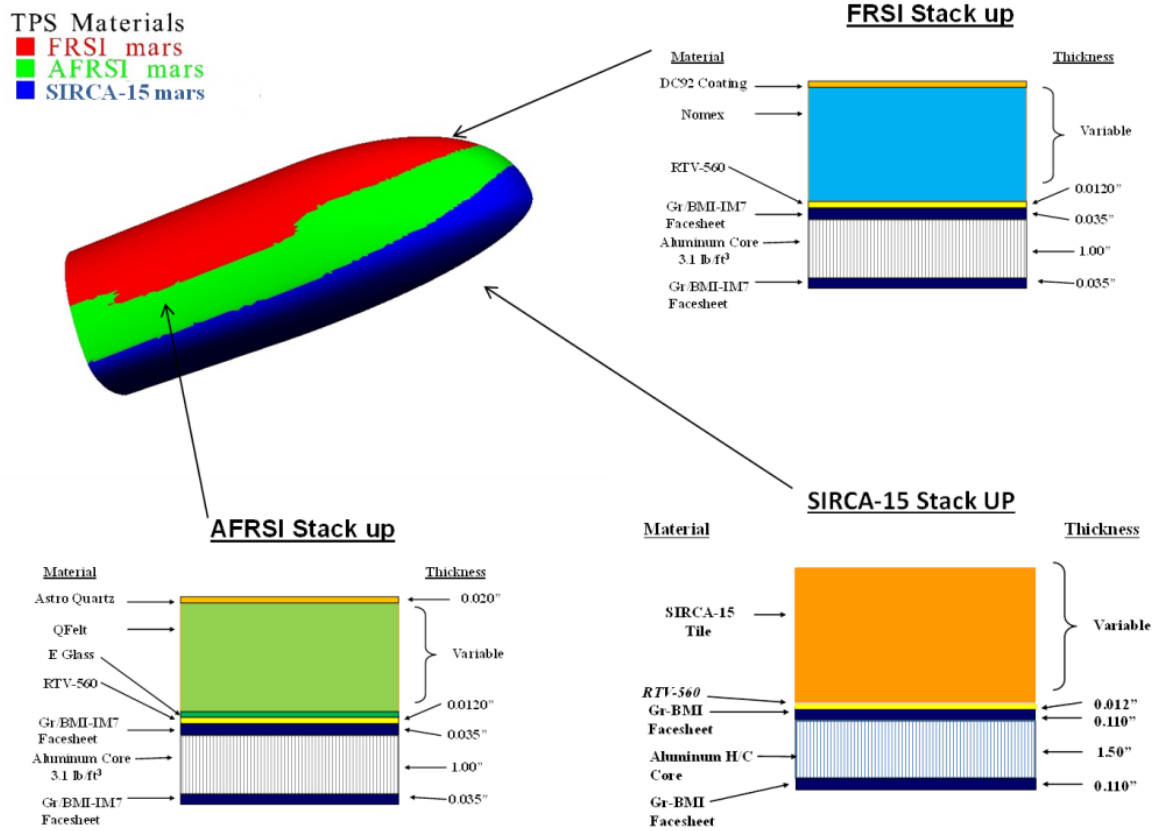


Figure 155. TPS Materials Stack-up.

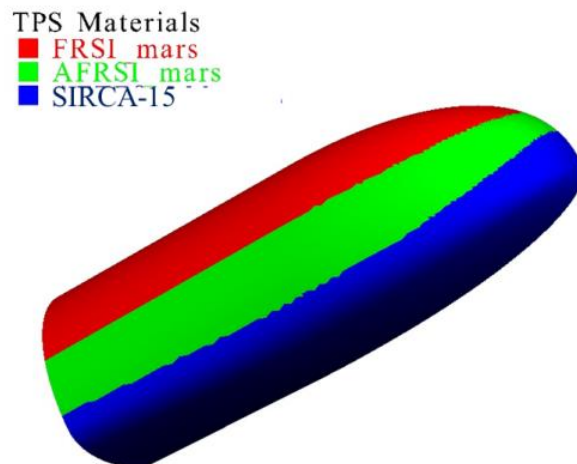


Figure 16. TPS Materials Distribution.

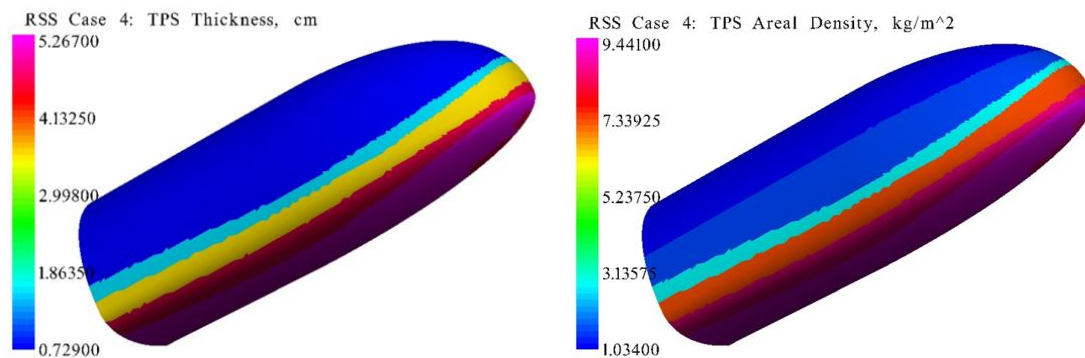


Figure 17. Selected TPS Thickness Distribution. Figure 18. Selected TPS Areal Density Distribution.

H. Other subsystems (Power, Thermal, C&DH, C&T, GN&C)

The power, thermal, guidance, navigation, and control equipment, command and data handling, and communications and tracking subsystems were sized with a common set of assumptions across the various entry concepts that were part of the EDL Architecture Study¹⁸. The combined dry mass of these subsystems is 1891 kg, or approximately 7.3% of the CobraMRV dry mass. The layout of these components within the aeroshell has a modest, but material impact on the location of the vehicle center of gravity.

As shown in Figure 5, the CobraMRV concept offers a substantial amount of available volume for mounting subsystem components around the perimeter of the cargo bay and in the nose region of the aeroshell. As a result of this flexibility, it is possible to place greater emphasis on operational and functional considerations such as line replaceable unit (LRU) accessibility, wire harness and fluid loop optimization, physical separation of redundant strings, and mass properties. The general layout plan for the CobraMRV is to locate the main avionics bays in the nose region along with the secondary batteries and the integrated power electronics (IPE). The forward landing gear will also be mounted in the nose bay. The fuel cell stacks will be located near the forward bulkhead of the payload bay to promote efficient integration with the propellant feed system and active thermal control loops. The aft landing gear will be mounted outboard on the aft ring frame near the inner mold line. Personnel resources were insufficient to pursue a detailed CobraMRV point design in 2016.

1. Power Subsystem

Under the current EMC architecture, the solar electric propulsion (SEP) stage provides power to the lander during the Earth-Mars transit. The SEP stage is jettisoned 48 hours prior to the aerocapture maneuver and the lander switches over to solid oxide fuel cells. The fuel cells consume methane and oxygen from the main propellant tanks to generate an average of approximately 7 kW during aerocapture and Mars orbit operations, with a peak of 16.4 kW during EDL. The fuel cells continue to provide an average of 10.7 kW of electrical power for up to 24 hours post-landing, by which point the ground power systems take over. The total energy generated by the fuel cells is approximately 340 kWh, which requires 42 kg of methane and 169 kg of oxygen. The lander power profile includes a 30% margin.

The integrated power electronics are based on a VERSA-Module Euro (VME) chassis with boards derived from the Orion Multi-Purpose Crew Vehicle (MPCV). In addition to providing redundant solar array switching, each IPE is capable of switching sixteen 4 A / 120 Vdc circuits, forty 1 A / 120 Vdc circuits, and eight 2 A / 28 Vdc circuits.

Under the multiple lander EMC architecture, the astronauts are delivered to Mars orbit in a separate vehicle using a rapid transfer trajectory. One lander remains in a 1 sol elliptical Mars parking orbit for up to a year, waiting to transport the astronauts down to the surface of Mars. UltraFlex solar arrays providing 100 m² of total area are deployed from the lander to generate electrical power during the extended Mars parking orbit phase. The current concept is that these solar arrays are jettisoned prior to deorbit.

2. Thermal Control Subsystem

Under the EMC architecture, the SEP stage does not provide thermal control to the lander. The CobraMRV is responsible for thermal control from Earth launch through EDL and during Mars surface operations. The current

CobraMRV concept includes two single-sided radiators (61 m² total radiating area) mounted on the inside of the payload bay doors to provide thermal control during the Earth-Mars transit and Mars orbit operations. Water sublimation is used to supplement the radiators for peak heat rejection needs, as well as to provide thermal control during aerocapture and EDL when the cargo bay door radiators are not available.

For the MAV payload, a pair of double-sided radiators providing 261 m² of effective radiating area are deployed post-landing at Mars to support ISRU generation and liquefaction of oxygen, maintain the liquid methane and oxygen in the MAV propellant tanks with zero boil-off, and provide general thermal control to operational lander systems. The area of the deployable Mars surface radiators will be sized to meet the needs of each payload configuration.

3. Command and Data Handling (C&DH) Subsystem

The primary functions of the C&DH subsystem are to provide command and control, data processing, and data storage and retrieval. A group of four single board computers (SBCs) with non-volatile solid state recorders is implemented in a Byzantine resilient architecture with full cross strapping to satisfy the fail operational/fail safe requirement. The flight computers utilize a time-space partitioned operating system and communicate over a time triggered network. A distributed avionics approach is employed to reduce the length and mass of sensor wire harnesses.

The precision landing and hazard avoidance (PL&HA) functions involve high speed processing of large quantities of sensor data during EDL for terrain relative navigation (TRN) and 3-D terrain mapping for hazard detection and avoidance (HDA). Given the uncertainties associated with predicting the capabilities of future space-qualified processors, a conservative approach was adopted in which a dedicated set of computers is included in the C&DH subsystem for the processing of PL&HA sensor data.

Common avionics are employed for the SEP, MAV, and lander to enhance the opportunities for the reuse and sparing of LRUs, as well as to offer the potential for increased levels of functional redundancy during mated mission phases.

4. Communications and Tracking (C&T) Subsystem

The C&T subsystem is designed to provide direct-to-Earth (DTE) communication links via a high gain dish antenna using X-band and Ka-band. Sensitivity trades between electrical power consumption, maximum data rate, and dish diameter have been performed. The maximum design bit error rate (BER) of the communications subsystem is 10⁻⁵ with a link margin of -3 dB or better. No assumption is made regarding the availability of communications relay satellites in Mars orbit. In the absence of orbital relay satellites, communications between the Mars base and Earth will occur in 12 hour on/off cycles.

The use of a high gain antenna places tight requirements on the pointing accuracy and stability of the host vehicle. In addition, multiple antenna boresight calibrations will be required to maintain communications performance during the long duration cruise. To avoid the anticipated scheduling difficulties associated with the DSN 70 m service, DSN 34 m is assumed for all mission phases except EDL. Even using DSN 70 m, however, the data rate during the EDL phase will be very low and is intended only for anomaly and/or accident analysis.

5. Guidance, Navigation, and Control (GN&C) Subsystem

The GN&C subsystem design is based on the application of proven tools and techniques for the development, analysis, testing, and certification of rigid entry body control systems blending active aerodynamic control surfaces and RCS thrusters. The core GN&C sensor suite is composed of high performance, flight proven inertial navigation sensors based on lessons learned from previous Mars missions, including Viking, Mars Pathfinder, MER, and MSL. A stable time reference and consistent time synchronization across the GN&C subsystem and sensor suite is required to support precision navigation and pointing. Sensor calibrations will be performed periodically during the mission and prior to each trajectory correction maneuver to ensure execution within a 0.1% (1 σ) magnitude error in delta-V and 3 mrad (1 σ) error in attitude. Slosh perturbations are expected to be well controlled by the design of the tanks and propellant management devices.

Ground-based navigation support from Earth includes orbit determination using DSN radiometric tracking data (S-band two-way range and 2/3-way Doppler) and nominal maneuver design. Position and velocity state vector updates will be uplinked periodically and prior to critical mission events. Maneuver information (burn times, magnitudes, and quaternions) will be computed on the ground and uplinked to the spacecraft. The GN&C subsystem design does not reflect any assumptions regarding the availability of other external navigation inputs, such as orbital

navigation satellites or surface beacons. If such assets are available, however, those measurements will be processed in the spacecraft navigation filter, as appropriate.

Precision landing is achieved by augmenting the core GN&C inertial sensor suite with highly accurate surface relative measurements, including terrain relative navigation and lidar-based altimetry and velocimetry. TRN provides map-based position updates through the correlation of real time terrain data obtained from onboard sensors with *a priori* reconnaissance data stored onboard the spacecraft, thus enabling early and efficient maneuvering to minimize global landing error and avoid large terrain hazards. Passive optical TRN utilizes commercially available, space-qualified cameras and optics, and was recently baselined on the NASA Mars 2020 and Resource Prospector missions. Passive optical cameras have the advantage of low mass and power relative to active sensors, but the mission design must provide adequate ambient lighting conditions along the EDL ground track. Active lidar-based TRN solutions are available if operation in darkness or near darkness is required.

Precision landing using orbital reconnaissance data enhances the probability of safe landing through the avoidance of identifiable hazards, typically a couple of meters in size or larger. Precursor missions can be employed to conduct detailed ground surveys to identify (or even prepare) areas free of hazardous slopes and surface roughness. Given that *a priori* knowledge, a controlled precision landing is equivalent to a safe landing. In the absence of high fidelity local maps, an autonomous, onboard hazard detection and avoidance system can be used to improve landing safety. The HDA system developed under the NASA Autonomous Landing and Hazard Avoidance Technology (ALHAT) project uses a gimbaled 3-D lidar sensor to rapidly generate a high resolution terrain map during the landing trajectory. After identifying and ranking the candidate landing sites, a small hazard avoidance maneuver is employed to position the lander for terminal descent. NASA JPL is currently studying the infusion of PL&HA functions on a Europa lander mission.

I. Mass Properties and Opportunities

Summary mass properties for the reference CobraMRV configuration are provided in Table 4. The CobraMRV has a gross mass of 61.1 mt, a dry mass of 26.1 mt, usable propellant of 14.4 mt, and a delivered cargo mass of 20 mt. The non-propellant category covers the thermal control fluids, pressurization fluids, propellant reserves and residuals, and fuel cell reactants that are commonly bookkept under inert mass. The mass growth allowance (MGA) percentages for each of the major dry mass categories are listed in Table 4. The effective MGA for the vehicle is 21.5%.

The single largest contributor to the CobraMRV dry mass is the structure at nearly 55%. The propulsion system is next at just over 20%, and the TPS is third at nearly 12% of the dry mass. The remaining 13.5% consists of power, thermal control, avionics, aerosurfaces, and mechanisms.

The usable propellant is calculated based on 650 m/s of delta-V for the main propulsion system at an effective specific impulse (Isp) of 360 seconds, and 255 m/s of RCS delta-V at an effective Isp of 325 seconds. The effective oxidizer to fuel mixture ratio (by mass) for the CobraMRV is 3.13. The main propulsion system uses a mixture ratio of 3.2. The RCS uses a more fuel-rich propellant mixture with a ratio of 3.0.

Early primary structural mass estimates for a basic CobraMRV aeroshell without cargo bay doors ranged from 6.3 to 6.7 mt. The mass estimates obtained from simplified finite element model (FEM) analyses were consistent with the results from other Pre-Phase A structural estimation techniques, such as simplified skin-stringer estimates and Mass Estimating Relationships (MERs). A subsequent FEM analysis using a non-load-bearing cargo bay door assumption (similar to the Space Shuttle Orbiter) and a more complete set of load cases yielded a mass estimate of 11.9 mt inclusive of the primary and secondary structure, plus attachment and support for the MAV and the CobraMRV descent engines and tanks. Including a 20% mass growth allowance (MGA), the 14.3 mt structural mass estimate represents approximately 55% of the total dry mass of the CobraMRV. At the current scale of the CobraMRV concept, each 1000 kg decrease in basic structural mass reduces the vehicle gross mass by 1560 kg, or roughly a 3:2 ratio. Of the additional 560 kg of vehicle gross mass reduction, approximately 360 kg comes from the reduction in propellant.

The structural FEM analyses include a 6.4 mm maximum skin deflection constraint based on rigid TPS design and flight experience. Since nearly two-thirds of the CobraMRV aeroshell is covered with flexible FRSI and AFRSI TPS, this deflection constraint may be somewhat conservative when applied to the entire vehicle. Analyses indicate that relaxation of the FEM skin deflection constraint to 12.7 mm may yield up to a 40% reduction in structural mass. However, until SLS minimum frequency constraints and other practical considerations are factored into the structural analyses, it is unclear to what degree the CobraMRV primary structure can be optimized.

The vehicle fineness ratio (length/diameter) also has a material impact on the structural mass. The reference CobraMRV concept was sized to maximize utilization of the SLS 10 m payload fairing with an 8.8 m diameter and 19.8 m length, or a fineness ratio of 2.25. From this starting point, FEM analysis has shown that a 1 m decrease in the length of the CobraMRV will result in a reduction in vehicle gross mass of roughly 1000 kg. This effect is non-linear, however, with the incremental mass benefit decreasing as the fineness ratio decreases. The effects of reducing the

fineness ratio on vehicle aerodynamics and stability and control have not yet been assessed, although it is clear that the ballistic number will rise because the reduction in drag area will outpace the reduction in entry mass. An increase in ballistic number will affect the CobraMRV EDL trajectory and, in turn, the total heat load and maximum heat flux. However, since the CobraMRV is operating well within the limits of SIRCA, the mass impact to the windward ablative TPS is expected to be small for modest changes in vehicle fineness ratio. An increase in ballistic number will also alter the altitude/velocity conditions at the transition from aerodynamic entry to powered descent and landing. Changes to the transition conditions will impact the amount of propellant required to perform powered descent.

The operational benefits of cargo bay doors were weighed against the inefficiencies of the large cargo bay door cutout in the primary structure, and two design alternatives were identified: load bearing, single-use cargo bay doors, and elimination of the cargo bay doors in favor of aft cargo extraction. Both of these design alternatives require the addition of articulated radiator panels to provide thermal control during the Earth-Mars transit and in Mars orbit. The design option employing a single use cargo bay door substitutes a pyro release system for the latching mechanism. The option eliminating the cargo bay doors requires the addition of a mechanical system for the aft deployment of a fully fueled MAV. Even so, it is anticipated that either of these alternatives will result in a substantial net mass advantage relative to the reference CobraMRV configuration.

The use of conventional structural materials for the reference CobraMRV design provides opportunities for mass reduction via the application of advanced composite materials and warm structure or hot structure. Mass savings can be achieved through the targeted application of advanced materials for skin panels, payload bay doors, and the aft access ramp, as examples. Given well defined load cases, a broader and more comprehensive application of advanced composite materials may yield somewhat larger structural mass reductions. Given a close match in thermal coefficient of expansion, the use of composite skin panels may enable direct bonding of the rigid windward TPS. This reduces TPS mass and complexity by eliminating the strain isolation pad and second layer of adhesive RTV. It may also be possible to eliminate gap fillers between TPS elements by reducing the size of the gaps. Depending on the choice of composite material for the skin panels, it may also be possible to increase the peak bond line temperature, thus reducing the TPS thickness and mass. Another option would be to eliminate the bonded TPS by employing a hot structure design, similar to the advanced carbon-carbon used on the Space Shuttle orbiter, or the carbon/silicon carbide used for the X-38 nosecone, fin leading edges, and split body flaps. Trade studies will be required to assess the relative cost, technical, and schedule risks of the various mass reduction opportunities for the CobraMRV.

The EMC ground rules specify the delivery of 20 mt of usable payload to the surface of Mars. However, the design of the payloads is affected by the mission load cases. In comparison to the low ballistic coefficient (HIAD and ADEPT) configurations, the Earth launch and Mars entry load cases for the CobraMRV are more challenging in terms of the variations in load paths. This is analogous to the launch, trans-Atlantic abort, and entry load cases for Space Shuttle payloads. The expectation is that this will result in a payload mass penalty that must be absorbed by the CobraMRV design in order to maintain equivalent payload performance with the other decelerator concepts. The magnitude of this payload mass penalty is unclear, and it is anticipated to vary with the type of payload.

In comparison to blunt body decelerator concepts with deployable drag devices, the rigid body CobraMRV is anticipated to have a higher gross mass for a given cargo capacity. Vehicle mass is an important design factor for any spacecraft, and is particularly critical for a landing vehicle that falls at the end of a chain of propulsive maneuvers. Vehicle mass impacts the ability of the SLS to deliver the CobraMRV and SEP stage to orbit, and a higher liftoff mass means a longer spiral out of Earth orbit and an extended Earth-Mars transit time. However, the higher gross mass of the CobraMRV concept must be weighed against the benefits of the configuration – mature materials, tools, and processes, proven flight control techniques, superior cargo protection, and potential advantages in terms of ground operations at Mars.

Table 4. Master Equipment List (System Level).

CobraMRV Cycle 1 Mass Properties			MGA	Mass (kg)	% Gross Mass	% Dry Mass
1.0	Structure		20.0%	14257	23.3%	54.7%
	1.1	Primary Structure		9624		36.9%
	1.2	Secondary Structure		4633		17.8%
2.0	Propulsion		24.1%	5263	8.6%	20.2%
	2.1	MPS		4046		15.5%
	2.2	RCS		1217		4.7%
3.0	Power		27.7%	1217	2.0%	4.7%
4.0	Avionics		23.7%	328	0.5%	1.3%
5.0	Thermal		25.0%	347	0.6%	1.3%
6.0	CobraMRV Systems		21.3%	4641	7.6%	17.8%
	6.1	TPS		3032		11.6%
	6.2	Aerosurfaces		260		1.0%
	6.3	Actuators		364		1.4%
	6.4	Landing Gear		985		3.8%
Dry Mass			21.5%	26052	42.6%	
7.0	Cargo			20000	32.7%	
8.0	Non-Propellant			684	1.1%	
Inert Mass				46736	76.5%	
9.0	Usable Propellant			14363	23.5%	
	9.1	MPS Usable Propellant		9448	15.5%	
	9.2	RCS Usable Propellant		4688	7.7%	
	9.3	MPS Engine Start/Stop Transient		227	0.4%	
Gross Mass				61099		

III. Conclusions

Design Analysis Cycle 1 for a rigid, human-scale, Mid-L/D vehicle optimized for Mars aerocapture and EDL has been completed. The CobraMRV design closes with margin at a gross mass of 61.1 mt and satisfies the EMC requirement to deliver 20 mt of cargo to the surface of Mars. The CobraMRV design leverages proven design and analysis tools and materials in addition to well-established validation, verification and certification processes for rigid entry vehicles. The CobraMRV also employs proven rigid body flight control techniques for aerocapture and EDL, combining active aerosurfaces with RCS thrusters to reduce the requirements for full scale flight testing. The emphasis on proven technologies and processes is expected to significantly reduce the technical, schedule, and cost risks of the CobraMRV development program relative to low ballistic number concepts augmented with deployable drag devices.

The CobraMRV shape is designed to maximize the benefits of aerodynamic drag and lift during the Mars atmospheric flight phases. The higher L/D provided by the slender body helps to offset the effects of the higher ballistic number resulting from the rigid body constraints on drag area. The higher L/D also increases hypersonic crossrange capability, provides control margin for load and heating alleviation, and enhances vehicle robustness to aerocapture and entry dispersions. The combination of aerodynamic shape, ballistic number, and L/D offered by the CobraMRV configuration has led to a reduction in the Mach number at SRP start as compared to previous Mid-L/D studies.

The CobraMRV aeroshell fully protects the cargo from the aerodynamic and aerothermal environments during aerocapture and entry, as well as the engine plumes and surface dust and debris generated during powered descent and landing. This comprehensive cargo protection can be extended throughout all flight phases by removing the in-space radiators from the inner surfaces of the PLB doors in favor of separate deployable panels. The CobraMRV concept also includes a large cargo bay, low deck height, and aft access ramp which are expected to provide superior operational flexibility on the surface of Mars in terms of cargo handling and ease of crew ingress and egress, both IVA and EVA. In contrast, taller, stacked lander configurations will likely require cranes and other specialized ground support equipment.

During Design Cycle 1, several opportunities for reducing vehicle structural mass were identified. Structural mass represents approximately 55% of vehicle dry mass, and each metric ton of dry mass that can be eliminated results in an additional savings of 300 kg of usable propellant. The structural efficiency of the CobraMRV aeroshell can be improved by either eliminating the PLB doors or by carrying loads through the PLB doors. Structural mass can also be reduced by shortening the aeroshell as long as the cargo dimension and volume requirements are still satisfied. Potential gross mass savings on the order of several metric tons or more is possible via design optimization, including tailoring of structural stiffness/deflection constraints. Advanced structural and TPS materials, including warm or hot structure carbon composites and advanced lightweight ablators, may offer additional mass savings at the expense of increased risk to vehicle development cost and schedule.

Refinements to the CobraMRV concept to be addressed in future studies include a detailed subsystems layout, SRP engine integration and performance, integration of key EMC cargo elements including the MAV and surface habitat, and SLS integration including stiffness, frequency, and loads constraints.

Additional forward work on the CobraMRV concept includes more detailed analyses of the mass reduction and design refinement strategies described above. The CobraMRV CAD model will be refined with more detailed subsystem and cargo layouts to reduce uncertainties in the vehicle mass properties. Finite element models will be matured to improve knowledge of the vehicle sensitivities to various design parameters. However, any changes to the CobraMRV OML will require a reassessment of the vehicle aerodynamics and aerocapture/EDL aerothermal environments. In 2017, a supersonic ballistic aerodynamics test is planned to help identify the aerodynamics and stability derivatives for the CobraMRV OML. The team will also continue to develop and refine the CobraMRV 6-DOF EDL trajectory simulation to explore trajectory performance, guidance design, vehicle stability, aerosurface and RCS usage, and landing performance, including the 50-m radius EMC landing precision requirement.

IV. Acknowledgments

The authors would like to acknowledge the contributions of the following team members who contributed to this study (in no particular order): Rhonda Moore, Dan Thomas, Mike Baysinger, Tara Polsgrove, Rick Rohan, Alicia Dwyer Cianciolo, Jamshid Samereh, D.R. Komar, Ellen Braden, Eduardo Llama, Stan Bouslog, Matthew Hershey, Jeff Hagen, Juan Barragan, Tim Collins, Jay Garcia, Jason Turpin, Jim Snoddy, Jack Chapman, John Peugeot, Steve Simpson, Bill Studak, Eric Hurlbert, Rob Morehead, Steve Sutherlin, Leo Fabisinski, Pat Loyselle, Glenn Rakow, Don Higbee, and Sharada Vitalpur.

V. References

- ¹Platoff, A., "Eyes on the Red Planet: Human Mars Mission Planning, 1952-1970", NASA/CR-2001-208928, July 2001.
- ²Braun, W., *Das Marsprojekt*, German 1st ed., Umschau Verlag, Frankfurt, 1952.
- ³Drake, B. G. (editor), "Reference Mission Version 3.0 Addendum to the Human Exploration of Mars: The Reference Mission of the NASA Mars Exploration Study Team", NASA Special Publication 6107-ADD EX13-98-036, June 1998.
- ⁴Hollis, B. R., Hollingsworth, K. E., "Experimental Aeroheating Study of Mid-L/D Entry Vehicle Geometries: NASA LaRC 20-Inch Mach 6 Air Tunnel Test 6966", NASA/TM-2014-218549, November 2014.
- ⁵Drake, Bret G., and Cooke, Douglas R. (Editors); "Reference Mission Version 3.0, Addendum to the Human Exploration of Mars: The Reference Mission of the NASA Mars Exploration Study Team"; Houston, Texas, 1998.
- ⁶Drake, B. G., "Human Exploration of Mars: Design Reference Architecture 5.0," NASA SP-2009-566, July 2009.
- ⁷Entry, Descent, and Landing Systems Analysis Study: Phase 1 Report, NASA/TM-2010-216720 (2010).
- ⁸Cianciolo, A. D., Polsgrove, T. T. "Human Mars Entry, Descent, and Landing Architecture Study Overview" SPACE 2016, AIAA 2016-5494
- ⁹Garcia, J.A., Brown, J. L., Kinney D. J., Bowles, J. V., et al., "Co-Optimization of Mid Lift to Drag Vehicle Concepts for Mars Atmospheric Entry," 10th AIAA/ASME Thermophysics Conference, 2010.
- ¹⁰Brown, J.L., Garcia, J.A., Kinney, D.J., Bowles, J.V., Mansour, N.N., U.S. Patent entitled "Co-Optimization of Blunt Body Shapes for Moving Vehicles" issued in 2014, Patent No.: US8725470
- ¹¹Matz, D. A., Lu, P., Mendeck, G. F., Sostaric, R. R., "Application of a Fully Numerical Guidance to Mars Aerocapture," (forthcoming).
- ¹²Berning, M. J., and McMiller, L., Programmer's Guide for the Simulation and Optimization of Rocket Trajectories (SORT) Program, Version 7, LESC-30423, October 1992.
- ¹³Ping Lu, "Entry Guidance: A Unified Method", *Journal of Guidance, Control, and Dynamics*, Vol. 37, No. 3, 2014, pp. 713-728.
- ¹⁴Gnoffo, P. A., "An Upwind-Biased, Point-Implicit Algorithm for Viscous, Compressible Perfect-Gas Flows," NASA TP-2953, Feb. 1990.
- ¹⁵Mazaheri, A., Gnoffo, P. A., Johnston, C. O., and Kleb, B., "LAURA User's Manual: 5.4-54166," NASA TM-2011-217092, May 2011.

- ¹⁶Johnston, C. O., Hollis, B. R., and Sutton, K., "Spectrum Modeling for Air Shock-layer Radiation at Lunar-Return Conditions," *Journal of Spacecraft and Rockets*, Vol. 45, No. 5, 2008, pp. 865--878.
- ¹⁷Johnston, C. O., Hollis, B. R., and Sutton, K., "Non-Boltzman Modeling for Air Shock Layers at Lunar Return Conditions," *Journal of Spacecraft and Rockets*, Vol. 45, No. 5, 2008, pp. 879--890.
- ¹⁸Cheatwood, F. M., and Thompson, R. A., "The Addition of Algebraic Turbulence Modeling to Program LAURA," NASA TM-107758, April 1993.
- ¹⁹Mazaheri, A., Johnston, C. O., and Sefidbakht, S., "Three-Dimensional Radiation Ray-Tracing for Shock-Layer Radiative Heating Simulations," *Journal of Spacecraft and Rockets*, Vol. 50, No. 3, 2013, pp. 485--493.
- ²⁰Kinney D., "Aerothermal Anchoring of CBAERO Using High Fidelity CFD," AIAA-2007-0608, 45th AIAA Aerospace Sciences Meeting and Exhibit, Reno NV, Jan. 2007.
- ²¹McGuire M. K., Bowles J., Yang L., Kinney D., Roberts C., "TPS Selection & Sizing Tool Implemented in an Advanced Engineering Environment," AIAA-2004-342, 42nd AIAA Aerospace Sciences Meeting and Exhibit